LUND UNIVERSITY

Large-Scale Retrieval of Coloured Dissolved Organic Matter in Northern Lakes Using Sentinel-2 Data

Al-kharusi, Enass Said.; Tenenbaum, David E.; Abdi, Abdulhakim M.; Kutser, Tiit; Karlsson, Jan; Bergström, Ann-kristin; Berggren, Martin

Large-Scale Retrieval of Coloured Dissolved Organic Matter in Northern Lakes Using Sentinel-2 Data

Enass Said. Al-Kharusi [1,*], **David E. Tenenbaum** [1], **Abdulhakim M. Abdi** [2], **Tiit Kutser** [3], **Jan Karlsson** [4], **Ann-Kristin Bergström** [4] **and Martin Berggren** [1]

[1] Department of Physical Geography and Ecosystem Science, Lund University, Sölvegaten 12, 22362 Lund, Sweden; David.Tenenbaum@nateko.lu.se (D.E.T.); Martin.Berggren@nateko.lu.se (M.B.)

[2] Centre for Environmental and Climate Research, Lund University, Sölvegatan 37, 22362 Lund, Sweden; hakim.abdi@cec.lu.se

[3] Estonian Marine Institute, University of Tartu, Mäealuse 14, 12618 Tallinn, Estonia; Tiit.Kutser@sea.ee

[4] Department of Ecology and Environmental Sciences, Linnaeus väg 6, 90187 Umeå, Sweden; Jan.P.Karlsson@umu.se (J.K.); Ann-Kristin.Bergstrom@umu.se (A.-K.B.)

[*] Correspondence: Enass.said@nateko.lu.se; Tel.: +46-700-29-62-69

Abstract: Owing to the significant societal value of inland water resources, there is a need for cost-effective monitoring of water quality on large scales. We tested the suitability of the recently launched Sentinel-2A to monitor a key water quality parameter, coloured dissolved organic matter (CDOM), in various types of lakes in northern Sweden. Values of $a(420)_{CDOM}$ (CDOM *absorption* at 420 nm wavelength) were obtained by analyzing water samples from 46 lakes in five districts across Sweden within an area of approximately 800 km^2. We evaluated the relationships between $a(420)_{CDOM}$ and band ratios derived from Sentinel-2A Level-1C and Level-2A products. The band ratios B2/B3 (460 nm/560 nm) and B3/B5 (560 nm/705 nm) showed poor relationships with $a(420)_{CDOM}$ in Level-1C and 2A data both before and after the removal of outliers. However, there was a slightly stronger power relationship between the atmospherically-corrected B3/B4 ratio and $a(420)_{CDOM}$ ($R^2 = 0.28$, n = 46), and this relationship was further improved ($R^2 = 0.65$, n = 41) by removing observations affected by light haze and cirrus clouds. This study covered a wide range of lakes in different landscape settings and demonstrates the broad applicability of $a(420)_{CDOM}$ retrieval algorithms based on the B3/B4 ratio derived from Sentinel-2A.

Keywords: Sentinel-2A; northern lakes; remote sensing; atmospheric correction; coloured dissolved organic matter (CDOM); water quality

1. Introduction

Long-term water quality information is important for securing and restoring ecosystem services provided by lakes [1]. Lakes are generally small in size and widely distributed in remote locations, which make regular monitoring difficult [2]. For example, Sweden has more than 126,000 lakes, but owing to the time and effort required to conduct monitoring with conventional sampling techniques, the annual Swedish lake monitoring program focuses on only around 100 lakes [3]. Similar challenges are faced by countries in northern boreal and Arctic regions that have an abundance of lakes scattered over large areas with low accessibility.

Water monitoring programs in Europe and North America have observed increases in dissolved organic matter (DOM) over the past decades [4], but knowledge of the geographic extent of these changes remains poor. DOM not only increases the cost of drinking water production and decreases recreational value of lakes, but also impacts the structure and function of aquatic ecosystems [5]

through, for example, degradation that leads to greenhouse gas production [5,6] and dissolved oxygen depletion [5–7], as well as decreases in light penetration, which suppresses biomass production [8,9]. As these impacts occur at large scales, there is an incentive to develop remote sensing techniques to map DOM in lakes of different sizes over large geographical areas with varying landscape settings.

The coloured fraction of DOM that absorbs light (CDOM) is conventionally described using a coefficient derived from the expression *ln(1/T)*, where T is the proportion (from 0 to 1) of photons transmitted through the CDOM in water per meter at a given wavelength [10]. In most aquatic ecosystems, quantifying CDOM is equivalent to knowing the absolute concentration of DOM in the water [11–13], although there can be local variations in the DOM/CDOM relationship [14]. As CDOM absorbs light and modifies the optical characteristics of the water, it can be remotely sensed from satellite observations [15]. Remote sensing can potentially provide new insights into how CDOM is spatially distributed in aquatic environments, and how it responds to climate and land-use change over space and time [15–17]. This facilitates effective monitoring of inland water CDOM [18] and the management of water resources, particularly if used in combination with in situ water sampling and monitoring programs [19].

Several sensors for environmental monitoring have been developed for marine applications (e.g., MODerate resolution Imaging Spectroradiometer, MODIS), but their coarse spatial resolutions, ranging from 250 m to 1200 m, are not suitable for most inland waters bodies [15,18,19]. Recently, the potential for inland water applications has been enhanced by the development of sensors with higher spatial and radiometric resolution [20–24]. The Sentinel-2 multispectral instrument (MSI) is a state-of-art sensor with freely available images at a spatial resolution of 10 m in the visible range that was designed for land applications, but with promising utility for monitoring regional lake water quality [25–27]. Furthermore, MSI includes 13 spectral bands, a swath width of 290 km, and global revisit times of five days with the twin satellites Sentinel-2A (launched in June 2015) and Sentinel-2B (launched in March 2017) [27].

There are several visible band ratio algorithms that can be used for estimating CDOM (and DOM) concentrations in a variety of lakes [15,28,29]. Most of these are based on the ratio between green and red bands because reflectance is low or negligible in the blue part of the spectrum in the majority of lakes owing to high absorbance by CDOM and/or interference from suspended particulate matter or phytoplankton [29,30]. For example, Toming et al. [29] found that CDOM in nine Estonian lakes followed a power function fitted to the ratio of MSI bands 3 and 4. However, the applicability of Sentinel-2 imagery in this regard is, thus far, largely unexplored and limited to small-scale studies. Furthermore, the extent to which a particular band ratio works for lakes of different sizes, CDOM ranges, topographical settings, and atmospheric conditions is poorly known.

This lack of knowledge calls for an explorative approach to evaluate the efficacy of different band ratios produced by this relatively new satellite to map CDOM at large scales. In this study, we evaluate retrieval algorithms for CDOM using Sentinel-2A MSI data for Swedish lakes with catchment areas that have a combined coverage of approximately 800 km^2, distributed across large parts of Sweden. Our research represents the first attempt to assess CDOM at such a large scale using Sentinel-2A data. Thus, the rationale behind our study is to test whether the performance of established CDOM retrieval methods using band ratios still holds at larger scales using Sentinel-2 data. We further discuss the importance of atmospheric corrections, pixel selection, and the handling of data outliers caused by atmospheric conditions.

2. Materials and Methods

2.1. Study Sites and In Situ Measurement

Forty-six lakes were sampled in five different districts in Sweden during the summer of 2016 (Tables 1 and 2, Figure 1). These are the *Norrbotten* subarctic unproductive landscape, which consists mainly of birch forest, shrublands, and bare rocks; *Västerbotten E*, which is characterized by a boreal

continuous spruce forest and peat wetlands; *Västerbotten W* and *Jämtland* districts, which have strong alpine gradients from lowland spruce to birch forest and further to high alpine conditions; and *Värmland*, which has a relatively productive boreal forest. All lakes were sampled more than once, but we decided to use data from visits close to dates with Sentinel-2A scenes that had minimum cloud cover. These lakes have no monitoring plan as they are relatively inaccessible, but the site selection was motivated by the need to test the performance of Sentinel-2A in regions where in situ data are rare.
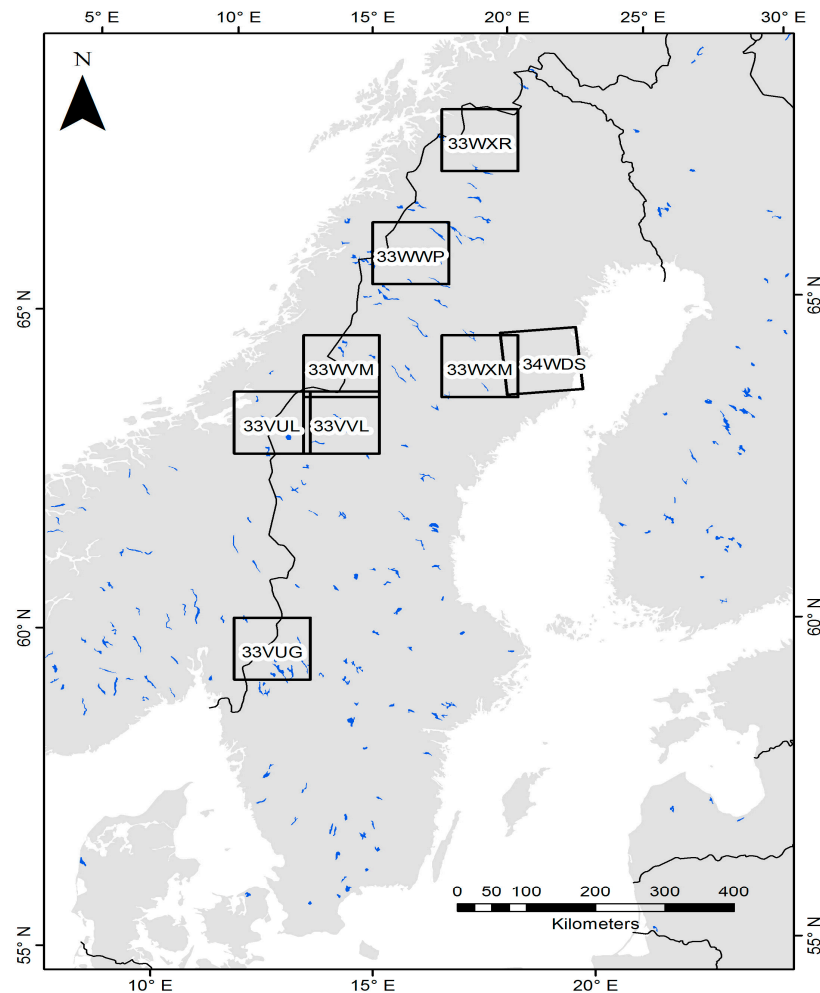
Figure 1. Locations of the five study regions in Sweden shown as Sentinel-2 tiles: *Norrbotten* (33WXR), *Västerbotten W* (33WWP), *Västerbotten E* (33WXM-34WDS), *Jämtland* (33WVM-33VUL-33VVL), and *Värmland* (33VUG).

Table 1. Descriptions of the land cover types in the Sentinel-2 tiles that cover the study area. *Norrbotten* (33WXR), *Västerbotten W* (33WWP), *Västerbotten E* (33WXM-34WDS), *Jämtland* (33WVM-33VUL-33VVL), *Värmland* (33VUG).

Sentinel-2 Tiles	Forest (Broadleaf and Coniferous)	Herbaceous	Wetland	Water
33WXR	35–82%	57–98%	10%	2%
33WWP	37–78%	55–95%	3%	1–11%
33WXM-34WDS	77–100%	11–98%	26%	1%
33WVM-33VUL-33VVL	25%	69–89%	3.5–7%	3–22%
33VUG	90–100%	3–5%	0	2–16%

Table 2. The identifier, name, region, and coordinates (midpoint) of each lake.

ID	Lake Name and Region	Latitude	Longitude
1	Skrapmiejaure-Västerbotten W	66°7′59.02″N	16°8′47.79″E
2	Aitelnastjärn-Västerbotten W	66° 6′17.87″N	16°11′5.28″E
3	Mattekjaure-Västerbotten W	66°7′3.34″N	16°11′11.27″E
4	Lissojaure-Västerbotten W	66°5′31.91″N	16°17′14.08″E
5	Tjappisjaure-Västerbotten W	66°4′5.96″N	16°21′10.36″E
6	Ruohtajavratje-Västerbotten W	66°5′11.45″N	16°19′22.67″E
7	Båsatjaure-Västerbotten W	66°7′18.87″N	16°15′55.72″E
8	Stor Bissitj-Västerbotten W	66°0′51.39″N	16°14′58.71″E
9	Övre Buonuokjaure-Västerbotten W	66°0′42.84″N	16°16′30.55″E
10	Nedre Buonuokjaure-Västerbotten W	66°0′32.77″N	16°16′15.05″E
11	Laddejaure-Jämtland	66°07′56.92″N	16°17′25.21″E
12	Avundtjärn-Jämtland	63°44′23.4″N	12°36′37.9″E
13	Svartvikstjärnarna-Jämtland	64°02′59.4″N	13°09′59.8″E
14	Krutejaure-Jämtland	63°55′20.2″N	13°27′00.0″E
15	Jille Skoulkenjaevrie-Jämtland	63°54′18.5″N	13°30′14.2″E
16	Baulan (Östra)-Jämtland	63°47′55.0″N	13°17′43.8″E
17	Jille Baulan (Västra)-Jämtland	63°47′58.9″N	13°16′57.4″E
18	Klingervattnet-Jämtland	64°37′16.4″N	14°34′44.7″E
19	Örtjärnen-Värmland	59°56′1.29″N	13°19′53.96″E
20	Hemsjön-Värmland	59°55′12.96″N	13°20′9.74″E
21	Igeltjärnen-Värmland	59°51′35.11″N	13°17′28.68″E
22	Göptjärnet-Värmland	59°53′4.93″N	12°44′46.53″E
23	Markustjärnet-Värmland	59°52′18.51″N	12°42′13.89″E
24	Stora Abbortjärnet-Värmland	59°50′48.60″N	12°38′48.93″E
25	Isakstjärn-Värmland	60°15′20.97″N	12°38′14.89″E
26	Djupen-Värmland	60°18′13.70″N	12°35′7.07″E
27	Hotlamm-Värmland	60°19′40.88″N	12°36′56.95″E
28	Stortjärnen-Västerbotten E	64°15′42.00″N	19°45′44.37″E
29	Enhörningen-Västerbotten E	64°15′2.39″N	19°3′1.35″E
30	Gäddtjärn-Västerbotten E	64°7′4.56″N	19°3′48.18″E
31	Övre Btj-Västerbotten E	64°7′24.34″N	18°46′44.35″E
32	Byxrivarlidvägen-VästerbottenE	64°7′31.28″N	18°45′18.37″E
33	Gålgotjärn-Västerbotten E	64°8′46.07″N	18°42′53.81″E
34	Nästjärn-Västerbotten E	64°9′1.26″N	18°48′0.51″E
35	Övre Skarda-Västerbotten E	64°13′19.64″N	18°50′48.72″E
36	Nedre Skarda-Västerbotten E	64°13′31.07″N	18°46′22.28″E
37	Mångstenstjärn-Västerbotten E	64°15′2.39″N	18°45′45.07″E
38	Banansjön-Norrbotten	68°26′43.24″N	18°37′44.70″E
39	Koukkelsjön-Norrbotten	68°26′33.21″N	18°34′38.94″E
40	Solbackasjön-Norrbotten	68°20′49.86″N	18°54′46.05″E
41	Hästskosjön-Norrbotten	68°21′1.55″N	18°58′3.08″E
42	Vouskojavri-Norrbotten	68°20′44.63″N	19°6′2.76″E
43	Långsjön-Norrbotten	68°20′15.96″N	19°8′46.65″E
44	Lillsjön -Norrbotten	68°19′57.79″N	19°8′44.80″E
45	Almberga-Norrbotten	68°19′54.46″N	19°9′10.69″E
46	Kaisepaktesjön-Norrbotten	68°15′53.85″N	19°24′22.73″E

A representative water sample was collected from each lake by sampling and pooling water from multiple depths (ca. 4–5 evenly distributed depths) within the mixed layer above the thermocline at the deepest point of the lakes. The water samples were kept cool until arrival at the laboratory, where samples were filtered (GF/F = 0.7 μm) and analyzed for absorbance using a Jasco V-560 UV/vis spectrophotometer (Easton, MD, USA). Filtered samples were refrigerated for up to one week after sampling before absorbance analysis. The measured absorbance values were converted to $a(420)_{CDOM}$ in Napierian units (based on a natural logarithm) with the equation $a(420)_{CDOM} = 2.303D/r$, where *D* is the measured absorbance and *r* is the cell path length (in m) [10,31]. Limnologists have used a variety of wavelengths to describe CDOM, and proposed 440 nm as a common standard in North American studies [10]. However, we used 420 nm as it is the wavelength used in the national Swedish monitoring program. The difference between the date of image acquisition and the corresponding in situ data collection ranged approximately between one week to ten weeks, potentially decreasing the

accuracy of our models [29]. However, past studies [15,32] have shown that CDOM concentration in lakes is a relatively stable parameter over these durations.

2.2. Satellite Image Processing

Level-1 Sentinel-2 MSI data (L1C) were downloaded from the Scientific Data Hub (https://scihub.copernicus.eu). A total of eight images from between June and October 2016 were downloaded, which covered all 46 lakes from the five different regions. Per-pixel radiometric measurements were provided as top-of-atmosphere (ToA) reflectance. The L1C products had been resampled with a constant ground sampling distance of 10, 20, and 60 m, depending on the native resolution of the different bands, and were delivered as scenes with UTM Zone 33N projection (WGS-84 datum). Images with 10 m and 20 m resolution were used [33]. Sentinel-2 Toolbox version 2.2.4 within the Sentinel Application Platform version 2.2.3 was used to process the images into Level-2A (L2A) surface reflectance using the Sen2Cor atmospheric correction module [33]. Sen2Cor is a processor used to generate Sentinel-2 L2A products, performing atmospheric, terrain, and cirrus cloud correction on the L1C data. Then, 3×3 pixel values were extracted from the middle of each lake and the mean values of the pixels were used for analyses. All processing was performed on a 64-bit Windows 10 workstation.

2.3. Statistical Analysis

Partial least squares regression (PLSR) was used to explore the relationships between lake CDOM concentrations and band ratios derived from Sentinel-2A bands 2, 3, 4, and 5 (Table 3). In this way, we were able to systematically evaluate and compare how accurate different ratios performed as CDOM predictors. Any ratio that was most strongly related to CDOM was then regressed against observed $a(420)_{CDOM}$ using power curves [29], which yielded the strongest relationships. A retrieval algorithm was then derived from the resulting regression model of different band ratios. Repeated *k*-fold cross-validation was performed in order to test the validity of the model. During this procedure, the data were divided into $k = 10$ portions of equal size, where one of these were retained for validation, while the rest $(k - 1)$ were used for training. The procedure was repeated five times to reduce variance. Model performance was assessed using the root-mean-square error (RMSE) and mean absolute error (MAE).

Table 3. Resolution, radiometry, and signal-to-noise ratio (SNR) of the Sentinel-2 bands used in this study.

Band	Resolution (m)	Central Wavelength (nm)	Region	Bandwidth (nm)	SNR
2	10	490	Blue	65	154
3	10	560	Green	35	168
4	10	665	Red	30	142
5	20	705	Red-Edge	15	117

3. Results

3.1. In Situ $a(420)_{CDOM}$ Measurements and Satellite Image Acquisition

The $a(420)_{CDOM}$ in the 46 lakes, as measured in the laboratory, varied from 0.30 m^{-1} to 29.93 m^{-1} (Table 4). The highest $a(420)_{CDOM}$ was recorded in seven lakes (IDs: 3, 24, 28, 30, 32, 33, 38) in Värmland and Västerbotten E with values between 21.2 m^{-1} and 29.9 m^{-1}. The clearest lakes were located in Västerbotten W, Jämtland, and Norrbotten, with observed $a(420)_{CDOM}$ between 0.4 m^{-1} and 2.4 m^{-1}. The reflectance of the lakes in the different regions was generally high in the green band (B3: 560 nm) and low in the red band (B4: 665 nm) (Figure 2).

Table 4. Dates of in situ sampling and image acquisition of Sentinel-2A, and the physical characteristics of the lakes.

| ID	Area (m^2)	Perimeter (m)	Sampling Date	$a(420)_{CDOM}$ (m^{-1})	Image Date
1	68,400	1980	28/07/2016	0.9	20/07/2016
2	136,800	2040	28/07/2016	0.52	20/07/2016
3	148,500	2220	28/07/2016	0.85	20/07/2016
4	376,200	3240	28/07/2016	0.97	20/07/2016
5	93,600	2760	28/07/2016	1.13	20/07/2016
6	209,700	3240	28/07/2016	1.42	20/07/2016
7	142,200	2280	28/07/2016	1.82	20/07/2016
8	117,900	2400	28/07/2016	0.85	20/07/2016
9	191,700	3120	28/07/2016	1.91	20/07/2016
10	238,500	2820	01/07/2016	1.14	20/07/2016
11	396,900	4080	24/08/2016	0.79	16/08/2016
12	279,900	3720	17/07/2016	1.02	05/09/2016
13	66,600	1620	17/07/2016	0.92	16/08/2016
14	218,700	2700	17/07/2016	2.4	16/08/2016
15	308,700	4740	17/07/2016	0.33	07/09/2016
16	227,700	3480	17/07/2016	0.3	07/09/2016
17	214,200	2760	17/07/2016	1.88	07/09/2016
18	341,100	5280	17/07/2016	1.78	07/09/2016
19	153,900	2520	09/07/2016	2.85	18/07/2016
20	251,100	3240	09/07/2016	0.55	18/07/2016
21	89,100	1620	09/07/2016	4.71	18/07/2016
22	32,400	720	11/07/2016	5.48	18/07/2016
23	48,600	1260	11/07/2016	8.22	18/07/2016
24	24,300	720	11/07/2016	9.21	18/07/2016
25	48,600	900	10/07/2016	4.06	18/07/2016
26	97,200	1980	10/07/2016	3.98	18/07/2016
27	340,200	3600	10/07/2016	2.29	18/07/2016
28	48,600	1080	12/07/2016	12.24	12/10/2016
29	129,600	1980	27/07/2016	2.93	21/07/2016
30	396,900	3780	27/07/2016	9.79	21/07/2016
31	56,700	1260	26/07/2016	13	21/07/2016
32	24,300	720	26/07/2016	10.62	21/07/2016
33	72,900	1620	27/07/2016	8.38	21/07/2016
34	24,300	720	26/07/2016	1.57	21/07/2016
35	40,500	1080	28/07/2016	5.29	21/07/2016
36	40,500	1080	28/07/2016	5.29	21/07/2016
37	56,700	1080	28/07/2016	4.97	09/10/2016
38	64,800	1980	25/08/2016	1.72	09/10/2016
39	40,500	1080	25/08/2016	1.42	09/10/2016
40	48,600	1080	23/08/2016	0.27	09/10/2016
41	72,900	1260	23/08/2016	0.8	09/10/2016
42	712,800	4680	23/08/2016	0.86	09/10/2016
43	137,700	2340	24/08/2016	0.14	09/10/2016
44	32,400	900	24/08/2016	0.82	09/10/2016
45	72,900	1260	24/08/2016	0.87	09/10/2016
46	2,770,200	12960	25/08/2016	0.4	09/10/2016
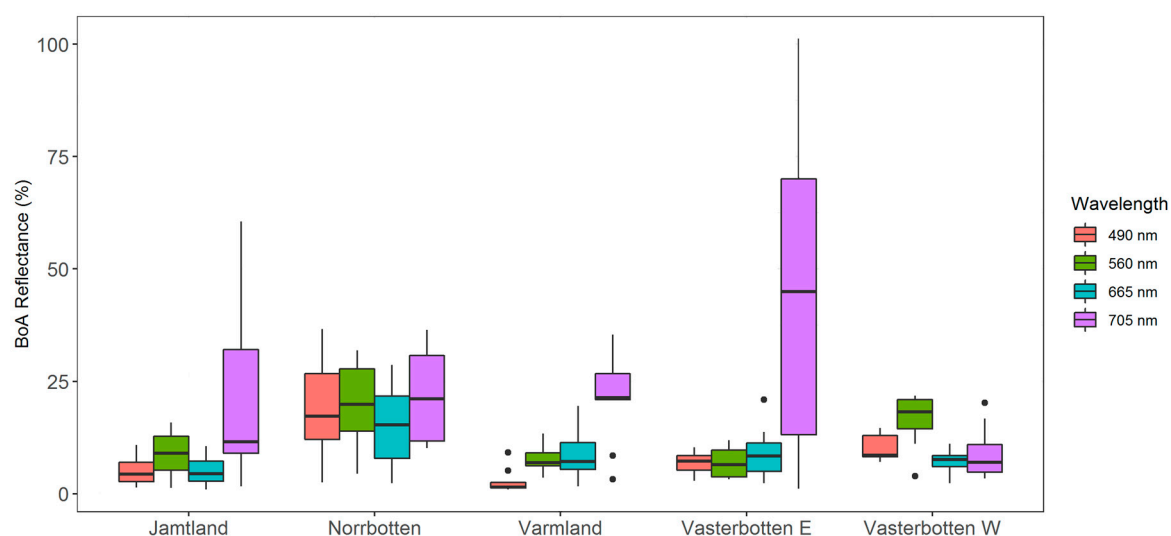
Figure 2. Reflectance spectra of 46 lakes in the five Swedish regions in this study. Reflectance values are bottom-of-atmosphere reflectance (BoA) after atmospheric correction. The wavelengths signify the central value in each band, as shown in Table 3.

3.2. Partial Least Squares Regression (PLSR) Model to Explore the Relationship between CDOM and Band Ratios

A PLSR analysis was used to explore the relationships between $a(420)_{CDOM}$ sampled in the lakes and the atmospherically-corrected band ratios. Two significant components were evident from the PLSR analysis. The first explained 40% of the variance in CDOM and was characterized by positive loadings weights for all band ratios. The second component explained that 34% of the variance in CDOM was characterized by positive loadings for ratios with B2 as the numerator, but with negative loadings for ratios with B3 as the numerator (Figure 3). The band ratio B3/B4 clearly showed the strongest relationship to $a(420)_{CDOM}$ as these two variables were located on the diagonally opposite end in the loading plot (Figure 3). The other band ratios, especially B2/B3, B2/B5, and B2/B4, were less clearly linked with $a(420)_{CDOM}$. The PLSR of the non-atmospherically-corrected L1C data (not shown) was excluded because of poor model fit.
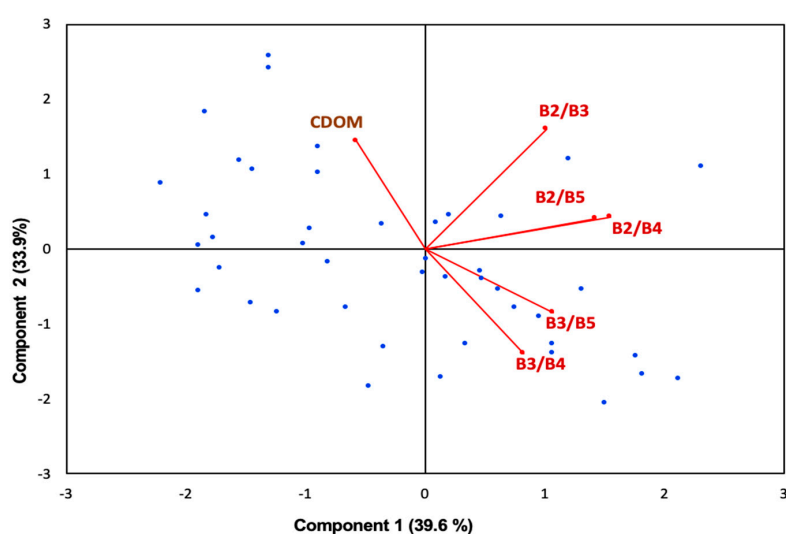

Figure 3. Partial least squares regression (PLSR) model with different band ratios variables as predictors (after atmospheric correction) and coloured dissolved organic matter (CDOM) as a response variable, based on data from 46 lakes in five different regions in Sweden. Vectors show loadings (PLS weights), scaled by a factor of 2 to fit the biplot with site scores. The site scores are shown in blue filled circles.

3.3. Testing and Validating a(420)$_{CDOM}$ Retrieval Models

The B2/B3 explained 24% of the $a(420)_{CDOM}$ variation before atmospheric correction (Figure 4A), but this relationship was not significant after atmospheric correction (Figure 4B). The green to red band ratio (B3/B4), which has been commonly used to retrieve CDOM in lakes in the past, had a relatively stronger correlation with the lake $a(420)_{CDOM}$ (Figure 4D). Before atmospheric correction, B3/B4 did not significantly explain any variance ($R^2 = 0.01$) in $a(420)_{CDOM}$ (Figure 4C), but after atmospheric correction the relationship was markedly improved ($R^2 = 0.28$; Figure 4D). The B3/B5 ratio showed patterns similar to those of B3/B4, but with slightly lower R^2 (Figure 4E,F).
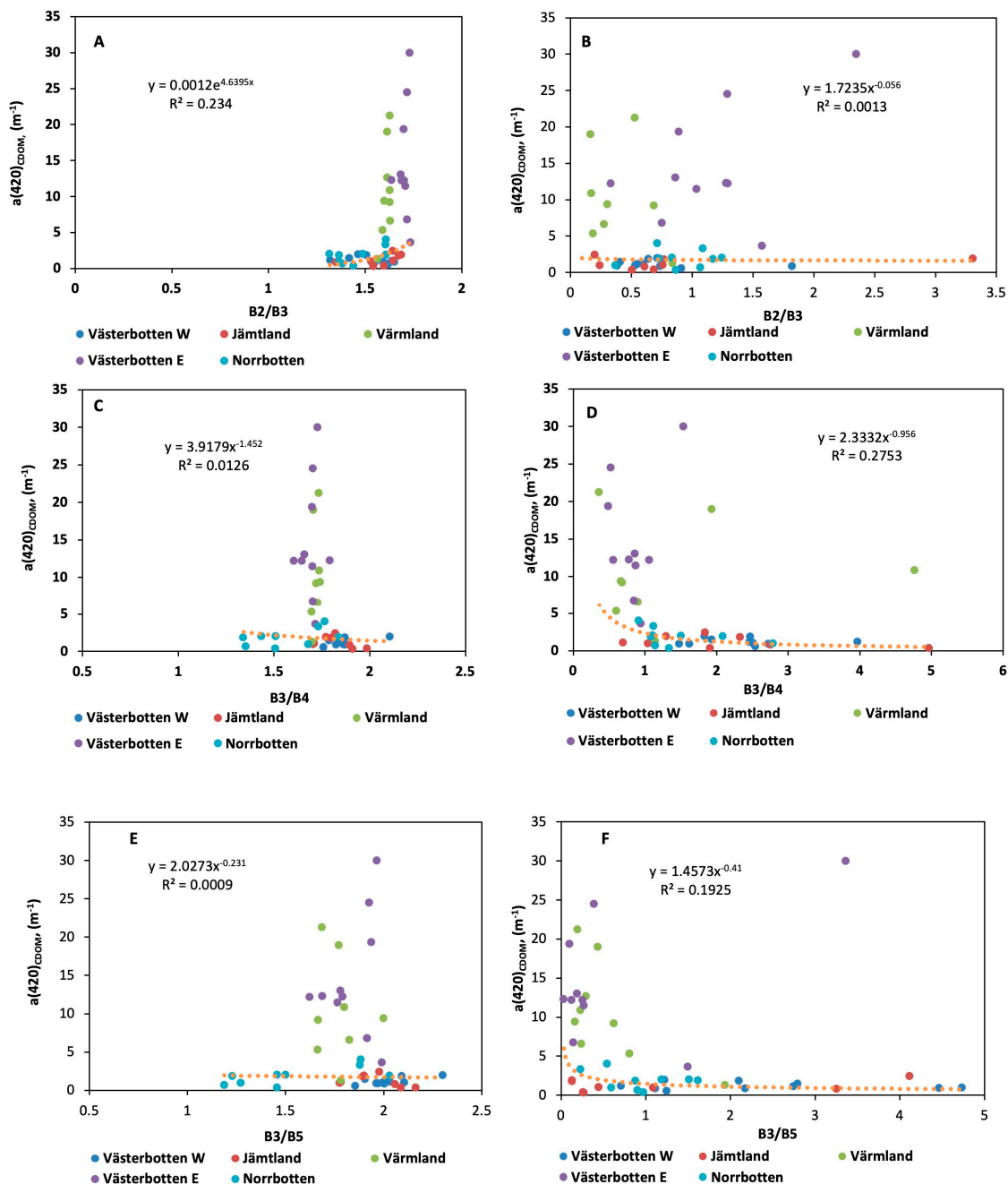

Figure 4. Relationships between ratio bands (B2/B3, B3/B4, B3/B5) calculated from Sentinel-2A data and in situ colored dissolved organic matter $a(420)_{CDOM}$ concentration measured: panels (**A,C,E**) are band ratios calculated from the top of atmosphere reflectance (L1C) data; and panels (**B,D,F**) are band ratios calculated from the bottom of atmosphere reflectance (L2A) data.

Model coefficients estimated from Sentinel-2A before (L1C) and after atmospheric correction (L2A) (Table 5) showed that B2/B3 had relatively higher explained variance and lower error and bias, in comparison with B2/B3 and B3/B5, before atmospheric correction. On the other hand, B3/B4 after the atmospheric correction showed the highest explained variance (R^2 = 0.28). Surprisingly, B3/B4 after atmospheric correction had slightly higher error and bias than B3/B4 and B3/B5 (Table 5).

Table 5. Retrieval models for $a(420)_{CDOM}$ estimated from Sentinel-2A before ([b], no shading) and after ([a], grey shading) atmospheric correction. RMSE, root-mean-square error; MAE, mean absolute error; the variable X denotes the band ratio in the model equation.

Band Ratio	Model	RMSE	MAE	R^2
B2/B3 [b]	$y = 0.0764 * X^{6.9008}$	1.0008	2.5384	0.2235
B3/B4 [b]	$y = 3.9179 * X^{-1.452}$	1.0563	2.9864	0.0126
B3/B5 [b]	$y = 2.0273 * X^{-0.231}$	1.0982	3.3289	0.0009
B2/B3 [a]	$y = 1.7235 * X^{-0.056}$	0.6412	1.9617	0.0013
B3/B4 [a]	$y = 2.332 * X^{-0.956}$	0.964	3.4234	0.2753
B3/B5 [a]	$y = 1.457 * X^{-0.41}$	0.6611	1.6376	0.1925

The repeated *k*-fold cross-validation showed that, after atmospheric correction, the B3/B4[a] ratio had the highest explained variance (R^2 = 0.49; Table 6). The RMSE showed substantially lower error and bias in B3/B4[a] in comparison with that found for other band ratios. This bolsters our confidence in using B3/B4 as a robust approach to predicting $a(420)_{CDOM}$ in lake water (Figure 5).

Table 6. The repeated *k*-fold cross-validation results of the performance of the Sentinel-2A band ratios for 46 lakes before ([b], no shading) and after ([a], grey shading) atmospheric correction.

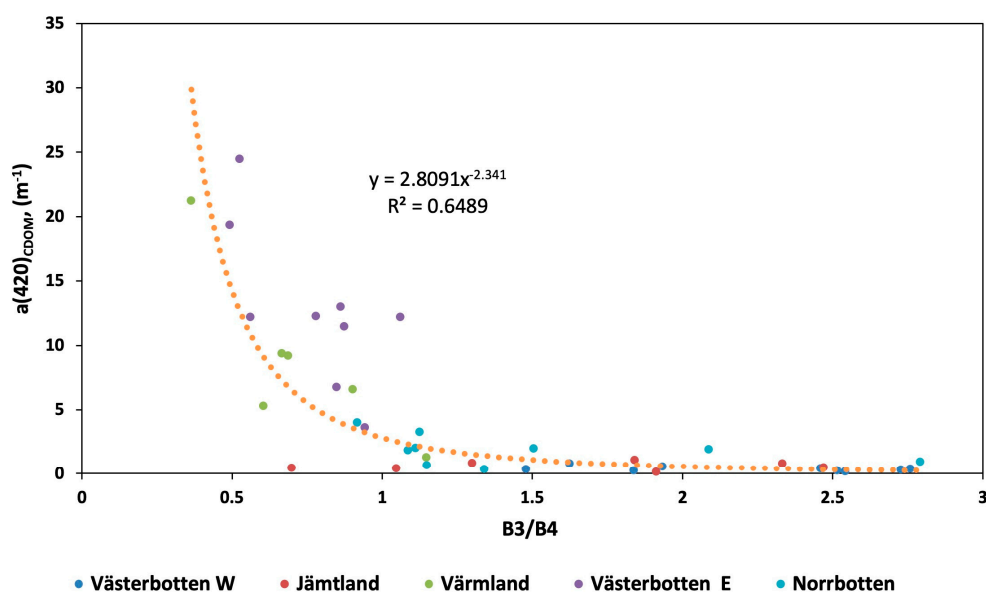| Band Ratio	RMSE	MAE	R^2
B2/B3 [b]	3.676	2.71	0.152
B3/B4 [b]	3.018	2.51	0.319
B3/B5 [b]	4.567	3.142	0.108
B2/B3 [a]	3.318	2.612	0.238
B3/B4 [a]	3.018	2.923	0.487
B3/B5 [a]	3.486	2.736	0.178

Figure 5. Power relationship between the CDOM absorption coefficient at 420 nm and the ratio of band 3 to band 4, calculated from Sentinel-2A data after the outliers were removed (n = 5), based on the results from 41 Swedish lakes.

The final model explained a relatively high proportion of the variance in CDOM (R^2 = 0.65) after the removal of outliers that were strongly affected by atmospheric conditions like haze and thin cirrus clouds (Figure 5). These outliers were not detected during the initial screening process in which we removed lakes that were completely covered by clouds because they had some cirrus clouds and haze that were harder to detect with the naked eye. Thus, they were removed in a secondary, and more detailed, inspection. As this study aims to test the efficiency of the MSI sensor for mapping CDOM concentrations at large scales rather than developing a new algorithm, we applied the final model from Table 7 to retrieve $a(420)_{CDOM}$ for the 41 lakes.

$$a(420)_{CDOM} = K \times \left(\frac{B3}{B4}\right)^{-m}, \tag{1}$$

where K is 2.809, $B3$ is centred at 560 nm, $B4$ is centred at 665nm, and m is –2.341.

Table 7. The best performing $a(420)_{CDOM}$ retrieval model estimated from the validation subset after atmospheric correction ([a]) and removal of outliers (n = 5). The variable X denotes the band ratio in the model equation.

Band Ratio	Model	RMSE	MAE	R^2
B2/B3 [a]	y = 1.9517 * X$^{0.2007}$	1.7095	1.3831	0.648
B3/B4 [a]	y = 2.8091 * X$^{-0.2.341}$	3.4834	1.09077	0.0076
B3/B5 [a]	y = 1.3702 * X$^{-0.615}$	6.4979	3.43316	0.2244

3.4. Comparing Observed and Modeled $a(420)_{CDOM}$ and Mapping Its Variability

Modeled and in situ, $a(420)_{CDOM}$ exhibited similar patterns and ranges across the study regions (Figure 6). Västerbotten E and Värmland had the highest $a(420)_{CDOM}$ concentrations and the highest variability. On the other hand, Jämtland and Norrbotten had the lowest variability in remotely sensed $a(420)_{CDOM}$ and clearer water compared with that of the other regions.
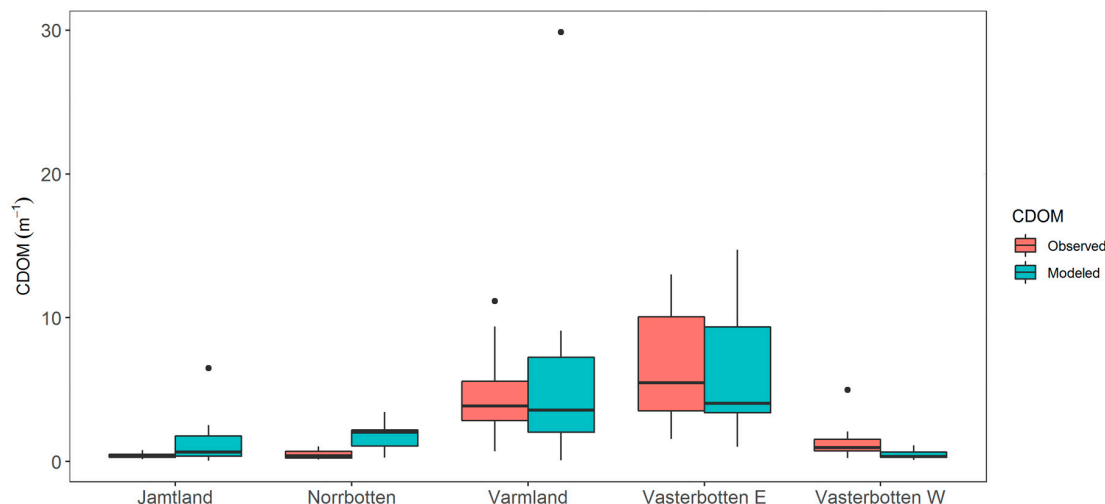

Figure 6. CDOM absorption coefficient at 420 nm, calculated from Sentinel-2A data and water sample, based on the results from 41 Swedish lakes.

The concentration of $a(420)_{CDOM}$ varied considerably within some of the lakes, as shown in Figure 7, where the spatial variation in $a(420)_{CDOM}$ of ten lakes in Västerbotten W is presented. For example, modeled $a(420)_{CDOM}$ was notably higher at the edges of several lakes compared with values derived from the middle pixels (Figure 7). On the other hand, for example, lakes 9–10 showed considerably less $a(420)_{CDOM}$ variability (Figure 7). In spite of this edge effect, the $a(420)_{CDOM}$ retrieval

also worked well in very small lakes. For example, one of the smallest lakes in the dataset (Lake 1, Skrapmiejaure), which is 0.07 km^2 in area, was still large enough for $a(420)_{CDOM}$ to be acquired (0–0.3 m^{-1}) from clean mid-lake pixels, owing to the high spatial resolution of the Sentinel-2A data.
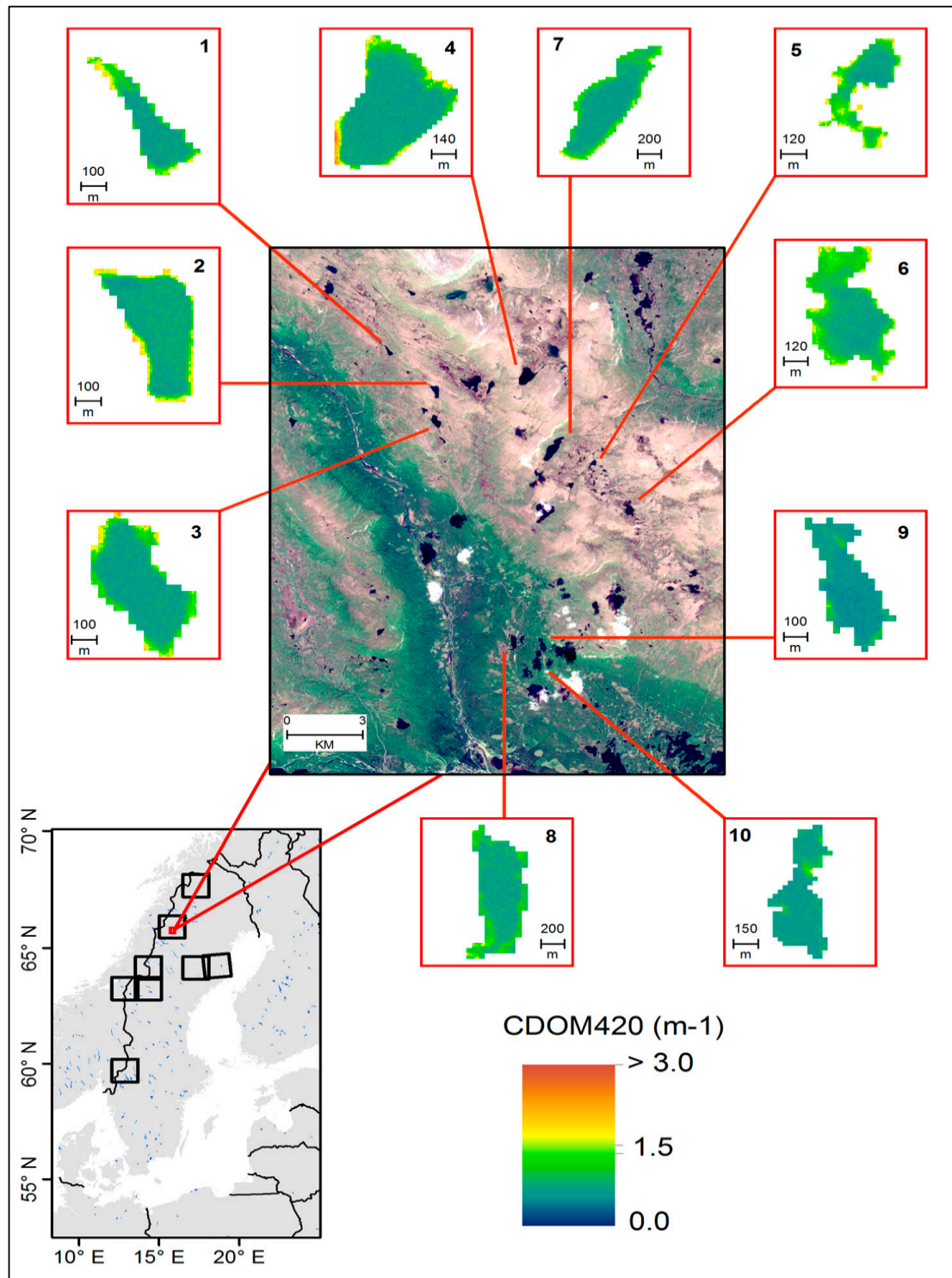

Figure 7. CDOM spatial gradient in lakes 1 to 10 covering Västerbotten W (33WWP). The base image in the central panel is Sentinel-2A true color composite taken on 21 July 2016. Note that Västerbotten W had some of the lowest in situ CDOM values (see Table 4 and Figure 5), which explains the low maximum in this figure.

4. Discussion

4.1. Band Ratio Algorithms

Several band ratio combinations were tested in this study and the B3/B4 ratio was found to perform best. In lakes with low CDOM concentrations, phytoplankton and other particles cause the green range (~560 nm, band 3) of the electromagnetic spectrum to reflect highly, while the red portion (665 nm, band 4) is mostly absorbed [17,34]. As CDOM increases, relatively more of the green light, as compared with the red light, will be absorbed, and thus relatively more red light, compared with green, remains available to be reflected back to the atmosphere (Figure 2). CDOM level may vary in the water columns, depending on the spectral interference from high concentrations of particulate matter (Figure 2). Zhu, W et al. [34] tested many empirical algorithms with lake data and suggested that wavelengths greater than 600 nm are critical for correct estimation of CDOM in complex freshwater ecosystems. In this study, we emphasize that the combination of the bands B3 and B4 in a ratio can capture the contrasting responses of these bands, and give a reasonable measure of $a(420)_{CDOM}$ content in the water.

The applicability of the Sentinel-2A data for estimating lake $a(420)_{CDOM}$ was highlighted by Toming et al. [29], who applied it to a relatively small area in Estonia. The primary limitation of their analysis is that the derived empirical relationship might only be valid for the small subset of lakes that were included in the study. We expanded the scope to include a much larger region and nearly three times the number of lakes and found a higher explained variance ($R^2 = 0.65$) for the relationship between $a(420)_{CDOM}$ and the B3/B4^a ratio than Toming et al. [29] ($R^2 = 0.52$). It is important to note that lake $a(420)_{CDOM}$ concentrations are influenced by several factors such as lake conditions, surrounding land cover and land use, topography, and atmospheric interference. In this regard, the strength of our approach is that the model developed involves a larger sample of lakes across a relatively larger spatial area with heterogeneous land cover and topography.

4.2. Atmospheric Effects

Generally, atmospheric correction must be applied to avoid unwanted illumination effects that may be larger than the variability in water parameters. However, Toming et al. [29] found that, for Sentinel-2A, the $a(420)_{CDOM}$ retrieval on small scale (single image) results were better when atmospherically uncorrected imagery was used. On a large scale, involving multiple images, we found that $a(420)_{CDOM}$ retrieval was more successful when atmospheric correction was applied to the imagery. We evaluated the added-value of using Sen2Cor by comparing the in situ and modelled $a(420)_{CDOM}$ before and after atmospheric correction using the B3/B4^a band ratios. On the basis of this analysis, we found that atmospheric correction worked well in general and the algorithm performance was evaluated using repeated *k*-fold cross-validation to obtain more reasonable estimates of model coefficients. As shown in Table 5, any differences in the spectra can lead to large differences in the absolute accuracy of band ratios retrieval of $a(420)_{CDOM}$. This can be explained in terms of biases and uncertainties that are dependent on spectral measurements of each band ratio.

Although we were not able to collect reflectance data in the field to compare it with the reflectance of acquired images, we were able to rate the performance of Sen2Cor by comparing the ToA and BoA reflectance spectra. We found that the reflectance spectra performed better in most regions after atmospheric correction. That being said, data from some sampling stations do not fit the general relationship well (Figure 4D). We investigated the specific images collocated with these sampling stations and found that there are residual signals in the blue and near-infrared wavelengths where water reflectance is supposed to be zero. This was because of persistent atmospheric effects, which indicate that either sun glint, light haze, or cirrus clouds were present, or potentially a combination of all of these conditions. Therefore, five lakes were removed from the dataset, and data from 41 lakes were used in the subsequent analyses (Figure 5).

4.3. Spatial Variability of a(420)$_{CDOM}$

In complex freshwater systems, $a(420)_{CDOM}$ often displays a broad range of values, likely influenced by catchment characteristics (e.g., vegetation type or density, or land cover variety). Such heterogeneous and often small lakes present a challenge to current remote sensing methods used to estimate biological and chemical properties of water [34,35]. Previous studies found that surrounding sources of carbon (e.g., vegetation, soils) enhance the $a(420)_{CDOM}$ values in lake water [36–40]. In our study area, specifically in Västerbotten E, wetlands are significantly represented in the total catchment area. Moreover, Västerbotten E and Värmland are dominated by a mix of broadleaf and coniferous forests, which could further explain the high values of $a(420)_{CDOM}$ in those regions (<5.5 to >10.5 m^{-1}; Figure 6, Table 4) [41,42]. On the other hand, Jämtland has the lowest percentage of forest and is mostly covered by herbaceous cover (Table 1). This could be the reason for the low $a(420)_{CDOM}$ levels found in this region (<2 m^{-1}, Figure 6 and Table 4) that cause more transparent water compared with other regions. Västerbotten W has a large proportion of mixed types of forest and herbaceous cover, which probably explains why $a(420)_{CDOM}$ at the edges of lakes in this region has high values in comparison with those found at lake centres. Depending on the size and depth of a lake and the heterogeneity of the topography, land cover, and land-use surrounding it, there could be a high variability of $a(420)_{CDOM}$ from the periphery to the lake centre. Therefore, it cannot be ruled out that lake bottom reflectance biases remote sensing measurements near the lake shore. Norrbotten has a mixture of different types of broadleaf forests and coniferous, herbaceous cover, and wetlands. The lakes in Norrbotten show a significant variation in $a(420)_{CDOM}$ (0.6–4.6 m^{-1}; Figure 6, Table 4). Overall, the lakes in areas surrounded by mixed forests had the highest levels of $a(420)_{CDOM}$, as compared with lakes surrounded by herbaceous vegetation or heathlands (Table 1). The contribution of different land cover types to the spatial patterns of $a(420)_{CDOM}$ in these lakes will be comprehensively assessed in a follow-up study (Supplementary Data; Figures S1 and S2).

4.4. Temporal Variability of a(420)$_{CDOM}$

The in situ $a(420)_{CDOM}$ measurements were obtained between July and August of 2016, and the Sentinel-2A images were collected in June, July, August, September, and October of the same year. Matching water sampling and satellite image acquisition in time was a challenge. The time difference was up to two weeks in all areas, except in boreal lakes in Västerbotten E; these had a difference in time of up to ten weeks.

Thus, a potential problem with our analysis is that there was a mismatch of up to approximately 10 weeks between the field sampling date and the date of the image that was available for analysis. However, Cardille et al. [32] suggested that a such a time difference will not significantly affect the relationship between measured and remotely sensed CDOM. In our case, the timing appeared to be sufficient for this study, and justified by the fact that our model was able to explain 65% of the variability in a(420)$_{CDOM}$, which is relatively high compared with other studies [29,30,43] that used Sentinel-2 data. The a(420)$_{CDOM}$ in boreal headwater lakes varies only marginally during the summer and we can expect relatively small temporal $a(420)_{CDOM}$ variations [44]. Weather conditions were stable during the study period, for example, maximum daily temperatures from June to September ranged between 18 °C and 25 °C, and precipitation was relatively low, between 25 and 45 mm. There were no heavy rain events between image acquisition and in situ data measurements that could bring particles or dissolved materials into the lakes, nor were algal blooms reported during the study period.

5. Summary and Conclusions

We presented an application of mapping lake coloured dissolved organic matter (CDOM) by modelling a(420)$_{CDOM}$ that may cause changes to water colour. In situ field measurements were taken from 46 lakes across northern Sweden during the summer of 2016 and eight images from the Sentinel-2A Multispectral Imager were acquired from the same season. Band ratios based on Sentinel-2A data were

used to model lake $a(420)_{CDOM}$. The best performing algorithm was based on the B3/B4 ratio, and it showed robust and consistent results across a broad range of lakes of different sizes distributed over varying landscapes. Sixty-five percent ($R^2 = 0.65$) of the variability of in situ CDOM was explained by the model. We found that atmospherically-corrected Sentinel-2 imagery produced better results than uncorrected imagery. However, we observed that the residual signal in atmospherically-corrected imagery may have been the result of sun glint, haze, or thin clouds that persisted despite the use of atmospheric correction. This study demonstrates the effective use of Sentinel-2 for this application over a wide range of inland waters that are situated in complex and inaccessible regions that are not well-monitored.

Supplementary Materials: The following are available online at http://www.mdpi.com/2072-4292/12/1/157/s1, Figure S1: Mapping 46 lakes in five study regions in Sweden using Sentinel-2 images; Västerbotten W (33WWP) acquired on 21 July 2016, Jämtland (33WVM-33VUL-33VVL) acquired on 30 July 2016, and Värmland (33VUG) acquired on 4 June 2016; Figure S2: Mapping 46 lakes in five study regions in Sweden using Sentinel-2 images; Västerbotten E (33WXM-34WDS) acquired on 12 October 2016 and Norrbotten (33WXR) acquired on 30 July 2016.

Author Contributions: The study was jointly designed by M.B. and D.E.T.; E.S.A.-K. was responsible for processing and analyzing Sentinel-2 imagery and wrote the manuscript with input from all co-authors; D.E.T. provided all technical support for the data analysis and contributed to the writing; A.M.A. helped in mapping CDOM and contributed to the writing; T.K. assisted in the processing data of Sentinel-2; J.K. supported to provide some of field data; A.-K.B. provided some of the field data; M.B., D.E.T. and A.M.A. assisted in writing in and enhancing the manuscript together with E.S.A.-K. All authors have read and agreed to the published version of the manuscript.

Conflicts of Interest: The authors declare there is no conflict of interest.

References

1. Birk, S.; Ecke, F. The Potential of Remote Sensing in the Ecological Status. Assessment of Coloured Lakes Using Aquatic Plants. *Ecol. Indic.* **2014**, *46*, 398–406. [CrossRef]
2. Verpoorter, C.; Kutser, T.D.; Seekell, A.; Tranvik, L.J. A Global Inventory of Lakes Based on High-Resolution Satellite Imagery. *Geophys. Res. Lett.* **2014**, *41*, 6396–6402. [CrossRef]
3. Fölster, J.; Johnson, R.K.; Futter, M.N.; Wilander, A. The Swedish monitoring of surface waters: 50 years of adaptive monitoring. *Ambio* **2014**, *43*, 3–18. [CrossRef]
4. Monteith, D.T.; Stoddard, J.L.; Evans, C.D.; De Wit, H.A.; Forsius, M.; Høgåsen, T.; Wilander, A.; Skjelkvåle, B.L.; Jeffries, D.S.; Vourenmaa, J.; et al. Dissolved Organic Carbon Trends Resulting from Changes in Atmospheric Deposition Chemistry. *Nature* **2007**, *450*, 537. [CrossRef]
5. Jansson, M.; Persson, L.; DeRoos, A.M.; Jones, R.I.; Tranvik, L.J. Terrestrial Carbon and Intraspecific Size-Variation Shape Lake Ecosystems. *Trends Ecol. Evol.* **2007**, *22*, 316–322. [CrossRef]
6. Lapierre, J.F.; Guillemette, F.; Berggren, M.; del Giorgio, P.A. Increases in Terrestrially Derived Carbon Stimulate Organic Carbon Processing and CO2 Emissions in Boreal Aquatic Ecosystems. *Nat. Commun.* **2013**, *4*, 2972. [CrossRef]
7. Brothers, S.; Köhler, J.; Attermeyer, K.; Grossart, H.P.; Mehner, T.; Meyer, N.; Scharnweber, K.; Hilt, S. A Feedback Loop Links Brownification and Anoxia in a Temperate, Shallow Lake. *Limnol. Oceanogr.* **2014**, *59*, 1388–1398. [CrossRef]
8. Karlsson, J.; Byström, P.J.; Ask, P.; Ask, L.; Persson, L.; Jansson, M. Light Limitation of Nutrient Poor Lake Ecosystems. *Nature* **2009**, *460*, 506. [CrossRef]
9. Deininger, A.; Faithfull, C.L.; Bergström, A.-K. Phytoplankton Response to Whole Lake Inorganic N Fertilization along a Gradient in Dissolved Organic Carbon. *Ecology* **2017**, *98*, 982–994. [CrossRef]
10. Cuthbert, I.D.; del Giorgio, P. Toward a Standard Method of Measuring Color in Freshwater. *Limnol. Oceanogr.* **1992**, *37*, 1319–1326. [CrossRef]

11. Brezonik, P.; Menken, K.D.; Bauer, M. Landsat-based Remote Sensing of Lake Water Quality Characteristics, Including Chlorophyll and Colored Dissolved Organic Matter (CDOM). *Lake Reserv. Manag.* **2005**, *21*, 373–382. [CrossRef]

12. Harvey, E.T.; Kratzer, S.; Andersson, A. Relationships between Colored Dissolved Organic Matter and Dissolved Organic Carbon in Different Coastal Gradients of the Baltic Sea. *Ambio* **2015**, *44*, S392–S401. [CrossRef]

13. Keith, D.J.; Schaeffer, B.A.; Lunetta, R.S.; Gould, R.W.; Rocha, K.; Cobb, D.J. Remote Sensing of Selected Water-Quality Indicators with the Hyperspectral Imager for the Coastal Ocean (HICO) Sensor. *Int. J. Remote Sens.* **2014**, *35*, 2927–2962. [CrossRef]

14. Song, K.; Zhao, Y.; Wen, Z.; Chong, F.; Shang, Y. A systematic examination of the relationships between CDOM and DOC in inland waters in China. *Hydrol. Earth Syst. Sci.* **2017**, *21*, 5127. [CrossRef]

15. Kutser, T.; Pierson, D.C.; Kallio, K.Y.; Reinart, A.; Sobek, S. Mapping Lake CDOM by Satellite Remote Sensing. *Remote Sens. Environ.* **2005**, *94*, 535–540. [CrossRef]

16. Kuster, T. The Possibility of Using the Landsat Image Archive for Monitoring Long Trend in Colored Dissolved Organic Matter Concentration in Lake Waters. *Remote Sens. Environ.* **2012**, *123*, 334–338.

17. Gholizadeh, M.; Melesse, A.; Reddi, L. A Comprehensive Review on Water Quality Parameters Estimation Using Remote Sensing Techniques. *Sensors* **2016**, *16*, 1298. [CrossRef]

18. Klein, I.; Gessner, U.; Dietz, A.J.; Kuenzer, C. Global WaterPack—A 250 m Resolution Dataset Revealing the Daily Dynamics of Global Inland Water Bodies. *Remote Sens. Environ.* **2017**, *198*, 345–362. [CrossRef]

19. Tyler, A.N.; Svab, E.; Preston, T.; Présing, M.; Kovács, W.A. Remote Sensing of the Water Quality of Shallow Lakes: A Mixture Modelling Approach to Quantifying Phytoplankton in Water Characterized by High-Suspended Sediment. *Int. J. Remote Sens.* **2006**, *27*, 1521–1537. [CrossRef]

20. Hakvoort, H.; De Haan, J.; Jordans, R.; Vos, R.; Peters, S.; Rijkeboer, M. Towards Airborne Remote Sensing of Water Quality in the Netherlands—Validation and Error Analysis. *ISPRS J. Photogramm. Remote Sens.* **2002**, *57*, 171–183. [CrossRef]

21. Arenz, R.F.; Lewis, W.M.; Saunders, J.F. Determination of Chlorophyll and Dissolved Organic Carbon from Reflectance Data for Colorado Reservoir. *Int. J. Remote Sens.* **1996**, *17*, 1547–1566. [CrossRef]

22. Jaffé, R.; McKnight, D.; Maie, N.; Cory, R.; McDowell, W.H.; Campbell, J.L. Spatial and Temporal Variations in DOM Composition in Ecosystems: The Importance of Long-Term Monitoring of Optical Properties. *J. Geophys. Res. Biogeosci.* **2008**, *113*. [CrossRef]

23. Sasaki, H.; Gomi, Y.; Asai, T.; Shibata, M.; Kiyomoto, Y.; Okamura, K.; Nishiuchi, K.; Hasegawa, T.; Yamada, H. Unique Dispersal of the Changjiang-Diluted Water Plume in the East China Sea Revealed from Satellite Monitoring of Colored Dissolved Organic Matter (CDOM). *Terr. Atmos. Ocean. Sci.* **2014**, *25*, 279–287. [CrossRef]

24. Palmer, S.C.J.; Kutser, T.; Hunter, P.D. Remote Sensing of Inland Waters: Challenges, Progress and Future Directions. *Remote Sens. Environ.* **2015**, *157*, 1–8. [CrossRef]

25. Drusch, M.; Del Bello, U.; Carlier, S.; Colin, O.; Fernandez, V.; Gascon, F.; Bargellini, P. Sentinel-2: ESA's Optical High-Resolution Mission for GMES Operational Services. *Remote Sens. Environ.* **2012**, *120*, 25–36. [CrossRef]

26. Baillarin, S.J.; Meygret, A.; Dechoz, C.; Petrucci, B.; Lacherade, S.; Tremas, T.; Isola, C.; Martimort, P.; Spoto, F. Sentinel-2 level 1 Products and Image Processing Performances. In Proceedings of the IEEE International Geoscience and Remote Sensing Symposium, Munich, Germany, 22–27 July 2012.

27. Salama, M.S.; Radwan, M.; van der Velde, R. A Hydro-Optical Model for Deriving Water Quality Variables from Satellite Images (Hydrosat): A Case Study of The Nile River Demonstrating the Future Sentinel-2 Capabilities. *Phys. Chem. Earth* **2012**, *50*, 224–232. [CrossRef]

28. Slonecker, E.T.; Jones, D.K.; Pellerin, B.A. The New Landsat 8 Potential for Remote Sensing of Colored Dissolved Organic Matter (CDOM). *Mar. Pollut. Bull.* **2015**, *107*, 518–527. [CrossRef]

29. Toming, K.; Kutser, T.; Laas, A.; Sepp, M.; Paavel, B.; Nõges, T. First Experiences in Mapping Lakewater Quality Parameters with Sentinel-2 MSI Imagery. *Remote Sens.* **2016**, *8*, 640. [CrossRef]

30. Kutser, T.; Paavel, B.; Verpoorter, C.; Ligi, M.; Soomets, T.; Toming, K.; Casal, G. Remote Sensing of Black Lakes and Using 810 Nm Reflectance Peak for Retrieving Water Quality Parameters of Optically Complex Waters. *Remote Sens.* **2016**, *8*, 497. [CrossRef]

31. Kirk, J.T.O. *Light and Photosynthesis in Aquatic Ecosystem*; Cambridge University Press: Cambirdge, UK, 1983.

32. Cardille, J.A.; Leguet, J.B.; del Giorgio, P. Remote Sensing of Lake CDOM Using Noncontemporaneous Field Data. *Can. J. Remote Sens.* **2013**, *39*, 118–126. [CrossRef]

33. ESA. SENTINEL-2UserHandbook. 2015. Available online: https://sentinel.esa.int\T1\ guilsinglrightdocuments\T1\guilsinglrightSentinel-2_User_Handbook (accessed on 24 July 2015).

34. Zhu, W.; Yu, Q.; Tian, Y.Q.; Becker, B.L.; Zheng, T.; Carrick, H.J. An Assessment of Remote Sensing Algorithms for Colored Dissolved Organic Matter in Complex Freshwater Environments. *Remote Sens. Environ.* **2014**, *140*, 766–778. [CrossRef]

35. Kallio, K.; Attila, J.; Härmä, P.; Koponen, S.; Pulliainen, J.; Hyytiäinen, U.-M.; Pyhälahti, T. Landsat ETM+ Images in the Estimation of Seasonal Lake Water Quality in Boreal River Basins. *Environ. Manag.* **2008**, *42*, 511–522. [CrossRef]

36. Li, J.; Yu, Q.; Tian, Y.; Becker, B.; Siqueira, P.; Torbick, N. Spatio-temporal variations of CDOM in shallow inland waters from a semi-analytical inversion of Landsat-8. *Remote Sens. Environ.* **2018**, *218*, 198–200. [CrossRef]

37. Kelly, P.T.; Solomon, C.T.; Weidel, B.C.; Jones, S.E. Terrestrial carbon is a resource, but not a subsidy, for lake zooplankton. *Ecology* **2014**, *95*, 1236–1242. [CrossRef]

38. Kritzberg, E.S.; Cole, J.J.; Pace, M.L.; Granéli, W.; Bade, D.L. Autochthonous versus allochthonous carbon sources of bacteria: Results from whole-lake 13C addition ex-periments. *Limnol. Oceanogr.* **2004**, *49*, 588–596. [CrossRef]

39. Boyle, E.S.; Guerriero, N.; Thiallet, A.; Vecchio, R.D.; Blough, N.V. Optical prop—Erties of humic substances and CDOM: Relation to structure. *Environ. Sci. Technol.* **2009**, *43*, 2262–2268. [CrossRef]

40. Williams, C.J.; Yamashita, Y.; Wilson, H.F.; Jaffé, R.; Xenopoulos, M.A. Unraveling the role of land use and microbial activity in shaping dissolved organic matter characteristics in stream ecosystems. *Limnol. Oceanogr.* **2010**, *55*, 1159. [CrossRef]

41. Maie, N.; Jaffé, R.; Miyoshi, T.; Childers, D.L. Quantitative and qualitative aspects of dissolved organic carbon leached from senescent plants in an oligotrophic wetland. *Biogeochemistry* **2006**, *78*, 285–314. [CrossRef]

42. Yallop, A.; Clutterbuck, B. Land management as a factor controlling dissolved organic carbon release from upland peat soils 1: Spatial variation in DOC pro-ductivity. *Sci. Total. Environ.* **2009**, *407*, 3803–3813. [CrossRef]

43. Chen, J.; Zhu, W.; Tian, Y.Q.; Yu, Q.; Zheng, Y.; Huang, L. Remote estimation of colored dissolved organic matter and chlorophyll—A in Lake Huron using Sentinel-2 measurements. *J. Appl. Remote Sens.* **2017**, *11*, 036007. [CrossRef]

44. Berggren, M.; Klaus, M.; Selvam, B.P.; Ström, L.; Laudon, H. Quality transformation of dissolved organic carbon during water transit through lakes: Contrasting controls by photochemical and biological processes. *Biogeosciences* **2018**, *15*, 457–470. [CrossRef]

Correction

Correction: Al-Kharusi, E.S., et al. Large-Scale Retrieval of Coloured Dissolved Organic Matter in Northern Lakes Using Sentinel-2 Data. Remote Sensing 2020, 12(1), p.157

Enass Said. Al-Kharusi [1,*] , **David E. Tenenbaum** [1] , **Abdulhakim M. Abdi** [2] , **Tiit Kutser** [3] , **Jan Karlsson** [4], **Ann-Kristin Bergström** [4] **and Martin Berggren** [1]

[1]   Department of Physical Geography and Ecosystem Science, Lund University, Sölvegaten 12, 22362 Lund, Sweden; David.Tenenbaum@nateko.lu.se (D.E.T.); Martin.Berggren@nateko.lu.se (M.B.)

[2]   Centre for Environmental and Climate Research, Lund University, Sölvegatan 37, 22362 Lund, Sweden; hakim.abdi@cec.lu.se

[3]   Estonian Marine Institute, University of Tartu, Mäealuse 14, 12,618 Tallinn, Estonia; Tiit.Kutser@sea.ee

[4]   Department of Ecology and Environmental Sciences, Linnaeus väg 6, 90187 Umeå, Sweden; Jan.P.Karlsson@umu.se (J.K.); Ann-Kristin.Bergstrom@umu.se (A.-K.B.)

*   Correspondence: Enass.said@nateko.lu.se; Tel.: +46-700-29-62-69

The authors wish to make the following correction to Table 7 in this paper.

The authors wish to declare that Table 7 of the originally published paper contains misprints, as data were inserted on the wrong lines by mistake. Additionally, one decimal period was inserted incorrectly. The correct Table 7 is shown in this correction paper. None of the results or conclusions of the study are affected.

Due to the misprints, replace:

Table 7. The best-performing a(420)$_{CDOM}$ retrieval model estimated from the validation subset after atmospheric correction ([a]) and removal of outliers (n = 5). The variable X denotes the band ratio in the model equation.

Band Ratio	Model	RMSE	MAE	R^2
B2/B3[a]	y = 1.9517* X$^{0.2007}$	1.7095	1.3831	0.648
B3/B4[a]	y = 2.8091* X$^{-0.2.341}$	3.4834	1.09077	0.0076
B3/B5[a]	y = 1.3702 * X$^{-0.615}$	6.4979	3.43316	0.2244

with

Table 7. The best-performing a(420)$_{CDOM}$ retrieval model estimated from the validation subset after atmospheric correction ([a]) and removal of outliers (n = 5). The variable X denotes the band ratio in the model equation.

Band Ratio	Model	RMSE	MAE	R^2
B2/B3[a]	y = 1.9517* X$^{0.2007}$	1.7095	1.3831	0.0076
B3/B4[a]	y = 2.8091* X$^{-2.341}$	3.4834	1.09077	0.648
B3/B5[a]	y = 1.3702 * X$^{-0.615}$	6.4979	3.43316	0.2244

The authors apologize for any inconvenience caused to the readers by these changes.

Reference

1. Al-Kharusi, E.S.; Tenenbaum, D.E.; Abdi, A.M.; Kutser, T.; Karlsson, J.; Bergström, A.K.; Berggren, M. Large-Scale Retrieval of Coloured Dissolved Organic Matter in Northern Lakes Using Sentinel-2 Data. *Remote Sens.* **2020**, *12*, 157. [CrossRef]